Doi: 10.1007/s11589-010-0735-5

Contemporary tectonic stress field in China*

Yongge Wan [1,2,♣]

[1] *Institute of Disaster-Prevention Science and Technology*, *Yanjiao*, *Sanhe* 065201, *China*
[2] *Institute of Geophysics*, *China Earthquake Administration*, *Beijing* 100081, *China*

Abstract The contemporary tectonic stress field in China is obtained on the basis of Chinese stress field database and Harvard CMT catalogue. Result of the inverted tectonic stresses shows that the maximum principal stress axis strikes nearly north-south direction in the west part of Tibet plateau, ENE direction in North China. In Central China, its strikes show a radiated pattern, i.e., NNE in north part and NNW in south part. The detailed stress field parameters of nearly whole China are given and can be used in geodynamic stress field simulation and earthquake prediction.

Key words: **tectonic stress field; focal mechanism; stress measurement**
CLC number: P315.72^{+}7 **Document code**: A

1 Introduction

Study of tectonic stress field, a major branch of Earth science, plays an important role in the studies of geodynamics. The World Stress Map Plan started in 1980s was led by M. L. Zoback. Lots of scientists participated in this plan. The plan collected global tectonic stress measurements and research results to establish global stress database. The world stress map was edited based on the global stress database. The world stress map reflects feature of global lithosphere stress field both in total and in subareas, and thus can explain the tectonic stress interaction in lithosphere (Zoback, 1992).

Tectonic stress field study has achieved significant development in China. In the early of 1970s, Li et al (1973) studied the stress field near a seismic station by synthetic first motion pattern of multi earthquakes (Aki, 1966). Xu et al (1983) extended this idea to stress determination by using multi- micro-earthquake and multi-station, further applied it to North China area. This method was also used to determine the tectonic stress field around Ordos block (Xue and Yan, 1984), East China (Wang and Xu, 1985) and Southwest China (Xu et al, 1987). Xu et al (1992) obtained the fundamental features of stress field in Chinese mainland by summarizing the stress field directions of previous studies, which reflects the close relationship between the motion of each block and that of the adjacent blocks. According to focal mechanism data and deep hole breakouts, Xu (2001) gave the present-day tectonic stress map for eastern Asia region. The maps of orientation of principal stress axes show that, apart from the strong influence of the collision between the Indian plate and the Eurasian plate, the present-day tectonic stress in eastern Asia is significantly affected by the back-arc extension of the subduction zones. The joint effect of the continental collision at Himalaya arc and back-arc extension in Myanmar arc region may be responsible for the remarkable rotation of principal stress orientations in southeastern part of Tibet plateau.

Another stress field determination method is using fault slip data and focal mechanism data (Angelier, 1979; Gephart and Forsyth, 1984; Michael, 1987). Based on stress determination method of Angelier (1979), Xu and Ge (1984) improved it and applied it to the 1931 *M*8.0 Fuyun, Xinjiang, earthquake. Using the similar method, the tectonic stress field in Southwest China (Xie et al, 1993; Cui and Xie, 1999) and in Guangdong and its adjacent areas (Kang et al, 2008) have been obtained. By using focal mechanism data in Chinese mainland, Du and Shao (1999) derived the tectonic stress field and principal stress ratio.

Nevertheless, neither Xu et al (1992) nor Du and Shao (1999) could cover their stress analysis on the whole China. For example, their stress analysis did not

* **Received** 9 April 2010; **accepted in revised form** 12 June 2010; **published** 10 August 2010.
♣ **Corresponding author. e-mail**: wanyg217217@vip.sina.com

cover most of Tarim basin, Ningxia Hui autonomous region, most part of Inner Mongolia autonomous region, Hubei and Hunan provinces, etc. However, the tectonic stress field in whole China is needed in some geodynamic and earthquake prediction study. For example, the load/unload response ratio method used to earthquake prediction needs to know the tectonic stress field in advance (Peng et al, 2000; Wan, 2004). In recent years, accumulation of stress measurement, fault slip measurement and focal mechanism data, especially establishment of crustal stress database in China and its adjacent areas (Xie et al, 2003), lays a solid foundation for the study on determination of Chinese tectonic stress field. By using this database, Xie et al (2004) summarized the fundamental features of Chinese tectonic stress field and divided the Chinese mainland into different tectonic stress blocks. In this study, we will divide the whole China into 2°×2° subregions and determine the tectonic stress direction and stress ratio in each subregion by using this database and CMT catalogue from 1976 to 2005.

2 Tectonic stress inversion method

Studying the state of stress in the Earth's crust and upper mantle is helpful in understanding plate motion and regional deformation (Hardebeck and Hauksson, 2001). Earthquake focal mechanisms are indicators of stress; thus, we will use earthquake focal mechanisms to detect stress state that cannot be directly measured. Several authors have proposed methods to determine orientations of stress axes of seismotectonic regime in spite of complicated tectonic settings (e.g., Gephart and Forsyth, 1984; Michael, 1984; Angelier, 1989; Horiuchi et al, 1995). For tectonic stress inversion is a nonlinear problem, Michael's method linearly determines the stress tensor by using least squares method and has a probability to trap in local minimum. So, in this paper, the focal mechanism stress inversion (short for FMSI) (Gephart and Forsyth, 1984) program by grid searching stress field parameters is used to determine the orientations of principal stress axes in China.

FMSI method has three basic assumptions (Gephart and Forsyth, 1984; Gephart, 1990): ① slip on the fault plane occurs in the direction of resolved shear stress, ② stress orientation is uniform in the calculated area, and ③ earthquakes are shear dislocations and can occur on preexisting faults. The FMSI method uses a grid search over stress field parameter space to find the best-fitting model that minimizes the average of the individual misfits between possible models and real data (Gephart and Forsyth, 1984; Gephart, 1990).

In FMSI, the individual misfit calculated for each earthquake is defined as the least rotation angle about any axis of general orientation which is needed to match the observed slip direction with one consistent with a given stress model (Gephart and Forsyth, 1984). We obtained the azimuths and plunges of three principal stresses axes σ_1, σ_2 and σ_3 ($\sigma_1 \geq \sigma_2 \geq \sigma_3$) and the ratio $R=(\sigma_2-\sigma_1)/(\sigma_3-\sigma_1)$ ($0 \leq R \leq 1$) by the best-fitting model. This may help us to distinguish the stress filed type.

There are four stress parameters (σ_1, σ_2, σ_3 and R) in the FMSI inversion algorithm, and the minimum number of events used to inversion is four. Moreover, diverse data set can give better constrains to find out the suitable stress tensor orientation. For above reasons, we used all the earthquake focal mechanisms within each data set to obtain an average local stress field without separating fault types in a region.

The procedure of FMSI to determine best-fitting stress model is as follows. We first perform a coarse initial grid search (with 10° spacing in stress orientations) covering the whole range of possible models for each data set by the approximate FMSI method (short for FMSIA, Gephart, 1990). We then take the best resulting stress model as a starting model to perform a fine grid search (with 5° spacing in stress orientations) by the exact FMSI method (short for FMSIE, Gephart, 1990).

In FMSI, the size of the average misfit corresponding to the best fitting stress model could be an indicator of the homogeneity degree of stress. According to a series of tests carried out by Wyss et al (1992) and Gillard et al (1996), for the real earthquake, focal mechanisms with errors of 15° (average of the uncertainties in strike, dip and rake) cannot obtain the average misfit of the stress inversion larger than 6°, thus the average misfit smaller than 6° may represent a homogeneous stress field. In contrast, the average misfit larger than 9° could be attributed to heterogeneity of stress. In the case of average misfit in the range between 6° and 9°, the stress solution is acceptable, but may reflect some heterogeneity (e.g., Wyss and Lu, 1995; Lu et al, 1997).

3 Data

The data used in Chinese tectonic field determination include: ① 918 focal mechanism data from 1920 to 2003 determined by Chinese scholars, ② 240 fault stria-

tion data from Quaternary fault slip measurements, ③ 72 stress relief data with all three axis directions at measured depth range of 50–363 m, and ④ 7 hydraulic fracturing stress data with all three axis directions at measured depth range from 400 m to 1 620 m. All the above data are from database of crustal stress in China and its adjacent areas (Xie et al, 2003). We also search the focal mechanism data from Harvard CMT solutions for the earthquakes in 1976–2005, which are not overlapped with the 918 focal mechanism data during 1920–2003 (Xie et al, 2003).

We divide the whole China into 2°×2° grids. In order to cover the whole study region and get the smoothing stress field, we select the data within the square areas of 5°×5° with the center of grid point. The stress field is smoothed by repeated selection of the focal mechanism data at different grid point, which looks more reasonable for stress field continuation. For the crust stress field has a probability different from the mantle stress field, we only select the data with depth less than 60 km. We cannot invert stress field in the areas less than four focal mechanism data, and use the stress direction determined by composite focal mechanism solution of Wang and Xu (1985) instead (Figures 1 and 2 quivers without color filled).

4 Results

Basing on the data above mentioned, we get the stress field nearly covering the whole China (Figures 1 and 2) by the stress field determination method (Gephart and Forsyth, 1984; Gephart, 1990) and the results are listed in Table 1. From Figure 1, we can see that the bigger misfit angles are distributed in east part of Tibet plateau, Tianshan and its west area, Taiwan and south-east costal region of China, showing larger heterogeneity of stress field (e.g., Wyss and Lu, 1995; Lu and Wyss, 1996; Lu et al, 1997). But the continuity of stress field with other areas shows the overall pattern may be accepted. From Figure 2, we can see larger number of focal mechanisms used in the inversion in Taiwan region, south-east coastal region of China, west to Tianshan region and central region of the Tibet plateau, which shows more constraint to these stress field results.

Table 1 Results of stress field inverted in this study

Lat. /°N	Long. /°E	σ_1 axis		σ_2 axis		σ_3 axis		R	Misfit angle /°	Number of earthquakes
		Az/°	Pl/°	Az/°	Pl/°	Az/°	Pl/°			
22	99	212	7	97	73	304	15	0.45	6.926	78
22	101	194	26	42	60	290	12	0.25	8.633	69
22	103	354	26	145	60	258	12	0.25	5.129	48
22	105	344	26	144	62	250	8	0.30	3.931	27
22	107	337	25	138	63	243	7	0.40	1.550	10
22	109	330	4	151	85	61	0			0
22	111	330	4	151	85	61	0			0
22	113	112	12	21	4	272	77	0.55	1.960	4
22	115	84	17	298	69	177	11	0.20	4.012	11
24	99	190	35	36	52	289	13	0.35	9.034	90
24	101	18	9	257	72	110	15	0.65	10.973	81
24	103	359	10	127	74	267	12	0.55	7.574	62
24	105	339	30	141	58	245	8	0.30	4.853	40
24	107	331	25	132	63	237	7	0.45	3.729	13
24	109	330	4	151	85	61	0			0
24	111	330	4	151	85	61	0			0
24	113	108	13	16	7	258	75	0.60	1.843	4
24	115	71	13	310	65	166	20	0.50	1.226	7
24	117	292	6	177	75	24	13	0.40	10.524	210
24	119	112	3	206	58	20	31	0.65	10.459	318
24	121	292	3	189	76	23	13	0.40	9.989	351
26	99	190	35	29	53	287	9	0.15	11.605	99
26	101	10	35	177	54	276	6	0.40	11.245	90
26	103	10	35	163	52	271	13	0.25	9.879	69
26	105	158	14	310	74	66	7	0.40	7.871	41
26	107	306	10	172	75	38	10	0.20	3.904	11
26	111	80	3	175	60	353	29			0
26	113	80	3	175	60	353	29			0
26	115	75	24	292	60	172	16	0.30	2.099	8

Continued from Table 1

Lat. /°N	Long. /°E	σ_1 axis		σ_2 axis		σ_3 axis		R	Misfit angle /°	Number of earthquakes
		Az/°	Pl/°	Az/°	Pl/°	Az/°	Pl/°			
26	117	112	4	221	78	21	11	0.45	10.029	143
26	119	99	9	213	68	6	19	0.40	10.914	246
28	85	178	14	299	64	83	21	0.40	5.393	40
28	87	188	34	343	53	90	12	0.40	5.471	39
28	89	188	34	20	55	282	6	0.50	7.282	58
28	91	25	14	205	76	295	0	0.70	9.115	66
28	93	39	7	144	64	306	24	0.95	10.821	81
28	95	39	30	205	59	306	6	0.75	10.589	85
28	97	180	50	39	32	296	20	0.50	11.272	104
28	99	182	55	40	28	300	18	0.50	12.105	85
28	101	10	35	179	54	277	5	0.40	12.726	79
28	103	10	35	157	50	268	16	0.35	13.290	57
28	105	123	23	321	65	216	7	0.70	10.506	38
28	107	293	18	49	53	192	30	0.65	2.790	10
28	109	320	5	226	33	58	56	0.10	0.738	4
28	111	80	3	175	60	353	29			0
28	113	80	3	175	60	353	29			0
28	115	69	14	330	29	181	57	0.50	0.442	4
28	117	296	3	192	77	27	12	0.40	9.818	96
28	119	110	9	211	50	13	38	0.65	9.432	196
28	121	110	9	213	55	14	33	0.60	9.889	220
30	81	15	5	225	84	105	3	0.50	3.869	27
30	83	174	26	317	58	76	16	0.20	4.795	34
30	85	186	30	354	59	93	5	0.35	5.566	60
30	87	348	61	191	27	96	10	0.50	5.787	62
30	89	293	81	23	0	114	9	0.85	5.429	70
30	91	269	81	13	2	104	9	0.50	6.758	78
30	93	203	66	32	23	301	3	0.50	9.463	88
30	95	48	43	200	43	304	14	0.65	9.660	68
30	97	240	85	27	4	118	3	0.70	9.484	81
30	99	248	55	93	32	356	12	0.10	9.413	72
30	101	79	66	291	20	197	12	0.60	12.469	66
30	103	293	39	119	50	26	3	0.65	9.951	48
30	105	118	32	278	56	22	9	0.50	9.313	37
30	107	293	18	49	53	192	30	0.65	2.769	12
30	109	272	7	181	0	86	83	0.70	1.189	5
30	111	273	1	14	84	187	5			0
30	113	77	66	249	23	159	0			0
30	115	69	7	233	82	339	2			0
30	117	47	14	311	19	170	66	0.75	0.996	4
30	119	249	38	96	48	350	14	0.40	5.530	10
30	121	282	83	94	6	185	1	0.40	5.488	21
32	79	17	7	227	81	108	4	0.70	8.558	47
32	81	183	19	338	69	90	8	0.20	6.646	40
32	83	178	14	315	71	85	12	0.40	6.004	47
32	85	183	23	357	66	92	2	0.35	6.170	70
32	87	186	30	341	57	89	11	0.40	6.194	70
32	89	200	60	1	28	96	8	0.30	7.183	84
32	91	203	66	7	23	100	6	0.35	7.693	93
32	93	240	80	30	8	121	5	0.60	7.675	88
32	95	45	35	184	47	299	21	0.60	9.177	67
32	97	45	35	184	47	299	21	0.60	11.555	77
32	99	69	35	245	54	338	2	0.30	12.522	59
32	101	69	35	245	54	338	2	0.30	10.841	52
32	103	281	9	20	46	183	42	0.90	12.630	46
32	105	294	2	26	47	202	42	0.50	9.529	36
32	107	297	19	51	49	194	34	0.60	3.140	12
32	109	96	0	5	69	186	21	0.80	0.683	6
32	111	273	1	14	84	187	5			0
32	113	77	66	249	23	159	0			0
32	115	252	12	34	74	160	9	0.40	0.516	5
32	117	257	7	139	75	349	13	0.50	0.397	5
32	119	252	12	34	74	160	9	0.40	1.065	6

Continued from Table 1

Lat. /°N	Long. /°E	σ_1 axis		σ_2 axis		σ_3 axis		R	Misfit angle /°	Number of earthquakes
		Az/°	Pl/°	Az/°	Pl/°	Az/°	Pl/°			
32	121	240	5	29	84	150	3	0.35	0.978	5
34	79	20	9	212	80	110	2	0.60	8.484	54
34	81	18	9	227	79	109	5	0.50	7.082	43
34	83	183	19	338	69	90	8	0.20	6.467	46
34	85	183	14	3	76	273	0	0.35	6.261	65
34	87	0	35	183	54	91	2	0.25	6.846	72
34	89	193	19	321	61	96	21	0.25	4.751	85
34	91	27	2	275	84	117	5	0.50	7.279	98
34	93	29	26	198	63	297	4	0.50	8.299	100
34	95	26	23	206	67	116	0	0.50	8.669	78
34	97	52	7	149	45	315	44	0.65	9.842	76
34	99	57	7	153	44	320	45	0.65	8.992	59
34	101	217	14	118	31	328	55	0.65	11.898	51
34	103	77	25	241	64	344	6	0.15	8.313	40
34	105	112	0	22	47	202	43	0.50	6.978	31
34	107	98	0	8	51	188	39	0.85	5.171	14
34	109	84	30	255	59	352	4	0.50	2.363	8
34	111	82	6	347	35	180	54	0.55	1.368	5
34	113	256	37	39	46	151	19	0.45	0.943	4
34	115	90	5	354	45	185	44	0.35	1.711	6
34	117	82	22	332	39	194	42	0.20	1.592	6
34	119	236	28	53	61	145	1	0.20	2.530	7
36	77	202	26	316	40	89	38	0.40	10.604	121
36	79	16	21	175	67	283	7	0.50	9.711	85
36	81	8	13	192	76	98	1	0.25	7.084	61
36	83	357	18	131	64	262	17	0.50	6.682	33
36	85	192	7	300	68	99	20	0.25	4.860	40
36	87	26	0	296	74	116	16	0.50	3.971	50
36	89	21	0	291	77	111	13	0.40	6.058	67
36	91	210	5	320	76	119	13	0.55	6.530	75
36	93	30	35	190	53	293	9	0.45	7.097	81
36	95	30	0	120	46	300	44	0.65	8.440	63
36	97	210	9	101	64	305	24	0.60	8.492	60
36	99	233	2	142	10	333	79	0.35	5.430	42
36	101	57	6	323	33	156	56	0.45	5.642	39
36	103	35	0	125	20	305	70	0.40	6.306	27
36	105	103	5	9	33	201	56	0.55	6.761	27
36	107	101	0	11	42	191	48	0.80	5.843	15
36	109	81	26	256	63	351	2	0.45	4.261	15
36	111	73	7	333	53	168	36	0.65	3.689	11
36	113	258	7	356	49	162	40	0.60	4.463	13
36	115	71	0	341	69	161	21	0.50	3.578	16
36	117	256	5	356	64	164	25	0.55	3.566	16
36	119	252	9	12	72	160	15	0.50	3.468	14
38	75	182	7	275	25	78	63	0.50	10.313	161
38	77	201	21	309	39	89	43	0.40	9.903	140
38	79	22	19	144	57	283	26	0.75	9.244	102
38	81	8	13	179	76	278	2	0.25	9.281	77
38	83	13	7	193	83	283	0	0.30	9.885	43
38	85	194	16	316	62	97	22	0.25	6.193	49
38	87	195	14	314	63	99	22	0.25	6.082	52
38	89	31	21	217	68	122	2	0.55	6.331	55
38	91	216	21	13	67	123	8	0.50	7.551	62
38	93	207	3	313	79	116	10	0.50	7.289	67
38	95	25	1	283	84	115	5	0.50	8.155	47
38	97	25	25	159	56	285	21	0.65	4.746	44
38	99	55	0	145	7	325	83	0.45	6.669	39
38	101	10	4	279	5	136	83	0.50	5.326	34
38	103	227	7	134	21	334	67	0.55	6.422	24
38	105	48	27	307	19	186	55	0.45	7.145	24
38	107	52	26	312	19	190	57	0.05	4.428	13
38	109	36	30	286	30	160	45	0.75	7.116	13
38	111	252	5	144	74	343	15	0.50	3.993	14

Continued from Table 1

Lat. /°N	Long. /°E	σ_1 axis		σ_2 axis		σ_3 axis		R	Misfit angle /°	Number of earthquakes
		Az/°	Pl/°	Az/°	Pl/°	Az/°	Pl/°			
38	113	77	0	167	65	347	25	0.45	5.677	15
38	115	255	4	353	65	163	24	0.55	3.829	17
38	117	255	4	353	65	163	24	0.55	3.552	16
38	119	271	26	36	50	166	28	0.75	3.644	13
38	121	257	18	46	69	164	10	0.50	3.324	11
38	123	255	9	117	77	346	8	0.40	3.632	9
40	75	187	18	96	2	357	72	0.40	9.082	143
40	77	22	14	153	69	288	15	0.45	9.387	123
40	79	196	26	307	36	80	42	0.55	9.377	101
40	81	10	5	220	84	100	3	0.20	9.639	81
40	83	208	14	112	22	328	63	0.15	9.015	47
40	85	198	14	308	54	99	32	0.20	8.710	34
40	87	193	14	309	60	96	25	0.30	8.294	32
40	89	210	9	335	74	118	12	0.50	8.104	35
40	91	44	0	134	34	314	56	0.40	8.196	38
40	93	41	0	131	30	311	60	0.40	7.477	40
40	95	41	0	131	30	311	60	0.40	6.624	37
40	97	198	9	359	80	108	3	0.15	7.043	40
40	99	217	7	307	3	67	82	0.30	5.407	35
40	101	198	21	45	66	292	10	0.40	6.529	30
40	103	207	14	71	70	300	13	0.50	5.995	22
40	105	28	31	269	38	144	36	0.70	7.142	23
40	107	40	24	192	63	305	11	0.10	7.854	12
40	109	69	36	250	53	159	1	0.25	5.081	13
40	111	83	4	182	66	351	23	0.60	3.604	16
40	113	73	7	315	75	165	13	0.55	2.357	17
40	115	255	4	352	60	163	29	0.50	3.901	18
40	117	258	18	144	51	0	33	0.30	3.033	17
40	119	87	14	206	63	351	22	0.35	2.839	14
40	121	87	19	214	60	349	22	0.25	2.627	11
40	123	87	19	214	60	349	22	0.25	1.046	8
42	81	351	0	261	4	81	86	0.35	7.101	70
42	83	7	13	99	9	226	74	0.50	3.737	35
42	85	2	7	93	13	245	75	0.65	3.945	24
42	87	2	7	94	22	256	66	0.65	4.624	23
42	89	12	2	102	9	271	80	0.70	3.962	22
42	91	12	2	102	9	270	80	0.70	5.813	23
42	93	45	9	312	17	161	70	0.25	5.910	30
42	95	23	14	118	22	263	63	0.55	6.033	26
42	97	23	14	117	17	257	67	0.55	4.924	23
42	99	200	5	290	7	76	81	0.35	5.263	23
42	101	28	14	238	73	120	8	0.25	5.408	19
42	103	34	31	231	57	129	8	0.75	3.762	11
42	105	66	31	228	57	331	8	0.25	5.414	14
42	107	85	0	175	75	355	15	0.80	5.493	11
42	109	87	9	197	66	353	22	0.65	4.535	13
42	111	83	7	191	68	350	20	0.60	3.553	15
42	113	243	19	79	70	335	5	0.35	4.994	15
42	115	252	2	344	53	161	36	0.45	2.829	17
42	117	87	14	222	70	354	13	0.45	4.328	17
42	119	252	2	344	53	161	36	0.45	3.759	14
42	121	252	2	345	58	161	31	0.40	3.242	12
42	123	252	7	353	58	158	31	0.40	2.048	9
42	125	62	14	275	73	149	10			0
42	127	62	14	275	73	149	10			0
44	81	186	18	290	37	76	47	0.50	7.928	67
44	83	358	9	88	4	203	80	0.55	5.929	33
44	85	8	14	100	9	222	73	0.50	3.994	28
44	87	192	7	284	18	82	70	0.60	3.776	23
44	89	192	7	284	18	82	70	0.70	4.057	20
44	91	192	2	282	17	96	72	0.65	3.616	16
44	93	196	17	83	50	298	34	0.65	6.306	17
44	95	14	0	284	21	104	68	0.65	3.896	11

Continued from Table 1

Lat. /°N	Long. /°E	σ_1 axis		σ_2 axis		σ_3 axis		R	Misfit angle /°	Number of earthquakes
		Az/°	Pl/°	Az/°	Pl/°	Az/°	Pl/°			
44	97	21	21	228	66	115	10	0.35	2.494	9
44	113	68	23	250	66	158	1	0.30	4.537	14
44	115	253	7	353	56	158	33	0.50	4.105	16
44	117	87	14	222	70	354	13	0.45	4.202	17
44	119	69	0	339	56	159	34	0.40	2.537	14
44	121	81	5	184	69	349	20	0.25	3.694	12
44	123	90	14	210	63	355	22	0.35	2.895	9
44	125	259	23	77	66	172	2			0
44	127	251	14	102	73	336	10			0
44	129	251	14	102	73	336	10			0
44	131	251	14	102	73	336	10			0
44	133	251	14	102	73	336	10			0
46	83	354	0	84	4	264	86	0.65	6.433	36
46	85	9	5	100	19	265	70	0.65	5.398	41
46	87	189	5	280	11	76	77	0.70	6.632	37
46	89	180	5	271	15	72	74	0.70	5.905	34
46	91	0	0	90	43	270	47	0.60	4.864	30
46	117	278	18	179	25	39	58	0.05	1.115	6
46	119	278	18	179	25	39	58	0.05	0.978	6
46	121	288	12	31	48	188	39	0.75	0.735	4
46	123	259	23	77	66	172	2			0
46	125	251	14	102	73	336	10			0
46	127	251	14	102	73	336	10			0
46	129	251	14	102	73	336	10			0
46	131	251	14	102	73	336	10			0
46	133	251	14	102	73	336	10			0
48	81	347	7	250	41	85	48	0.50	3.889	13
48	87	355	0	265	20	85	70	0.65	6.147	31
48	117	288	12	31	48	188	39	0.75	0.735	4
48	119	277	18	177	26	37	57	0.05	0.481	4
48	121	90	9	199	64	356	24	0.50	0.842	4
48	123	259	23	77	66	172	2			0
48	125	259	23	77	66	172	2			0
48	127	251	14	102	73	336	10			0
48	129	251	14	102	73	336	10			0
48	131	251	14	102	73	336	10			0
50	121	259	23	77	66	172	2			0
50	123	259	23	77	66	172	2			0
50	125	259	23	77	66	172	2			0
50	127	251	14	102	73	336	10			0
52	119	58	14	176	62	322	23	0.50	2.238	5
52	121	60	35	213	52	321	13	0.20	0.688	4

Note: The data with Number of earthquakes of 0 are from Wang and Xu (1985).

Most of σ_1 and σ_3 axes are horizontal (Figures 1 and 2), indicating that the seismotectonic deformation takes place primarily through strike-slip faulting. The continuous σ_1 and σ_3 direction showing the stress field in China and its adjacent areas has the same source which is driven by the northward indentation of the Indian plate, and subduction of the Pacific ocean plate under the Eurasia plate. The western part, i.e., Tibetan plateau, undergoes north-south compression and east-west extension, and this trend extends to Xinjiang area. The σ_1 direction appears to curve sharply in the eastern end of Himalaya arc, showing some eddylike feature to the south of the Assam wedge (Figure 1). The principal stress axes show a relatively uniform radial pattern. That is, the compressive horizontal stress trajectories radiate from Tibet plateau to the northern, eastern, and southeastern parts of the mainland (Figure 1). The inferred extensional stress directions lie along arcs convex outward from the plateau (Figure 2). Despite inevitable local variations, which are often indistinguishable from the error in stress axis estimation, this overall pattern is schematically expressed in Figure 1 by horizontal stress trajectories.

In central part of Tibet plateau, there are relative vertical σ_1 axes, horizontal σ_3 axes in east-west direction. This may be caused by the extension of this region and

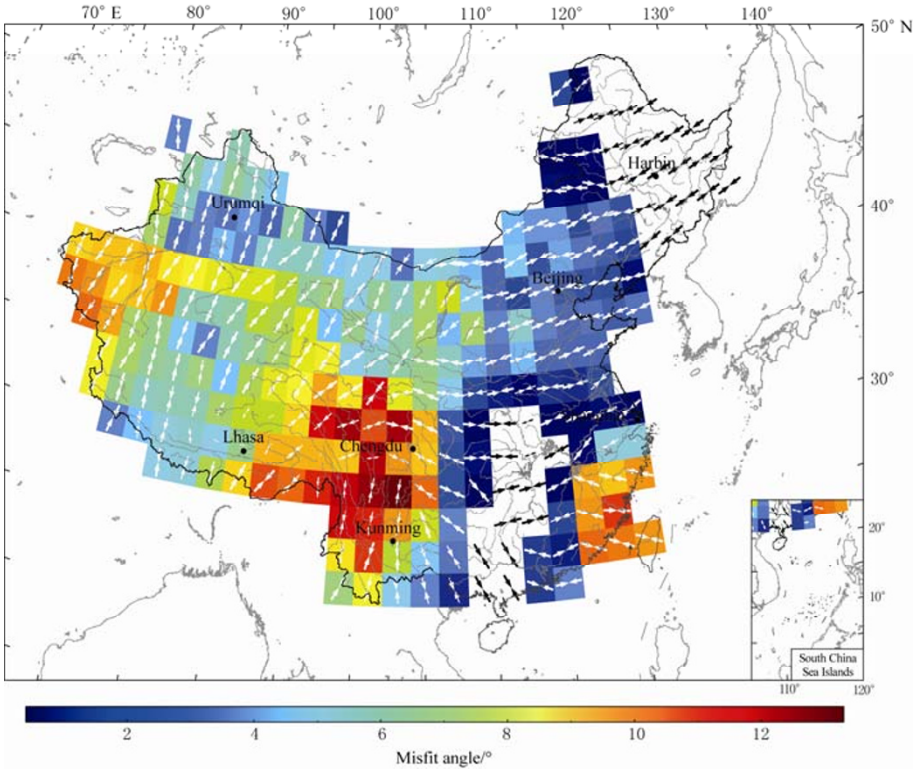

Figure 1 σ_1 direction and misfit angles obtained in this study. Quivers show the directions of σ_1, and the longer the quiver is, the more horizontal the σ_1 will be.

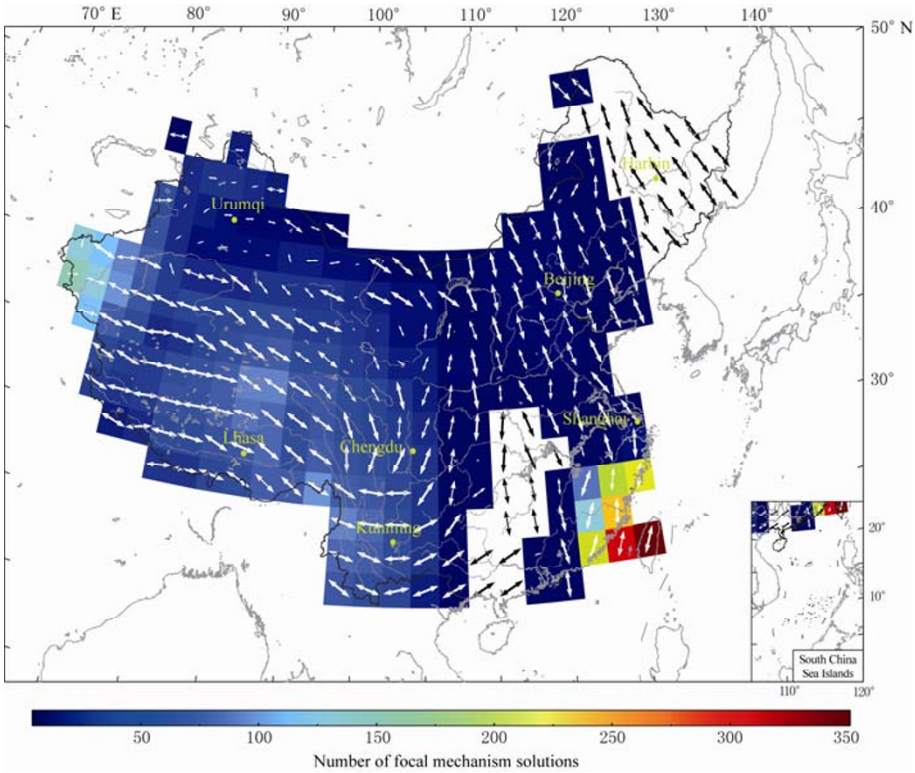

Figure 2 σ_3 direction and number of data used in this study. Quivers show the directions of σ_3, and the longer the quiver is, the more horizontal the σ_3 will be.

be validated by more lakes in this area. In the North-South Seismic Zones, we can see that the stress direction changes sharply, which indicates a dividing line of the stress field in this area.

5 Discussion and conclusions

The data used to infer modern stress field in the present study come from earthquakes occurred during the past several decades, stress measurements in recent years and quaternary fault slip measurements. It is interesting to notice that a similar pattern of stress axes as discovered in this study has also been found before. For example, Xu et al (1992) used a different method to get the mean principal tress axes basing on 9 621 P wave first motion polarity from 5 054 small earthquakes. Using the similar method to this study, Du and Shao (1999) also got the modern tectonic stress field. Based on the data of earthquake centroid moment tensor (CMT) solution, P-wave first motion focal mechanism solution and deep hole breakouts, Xu (2001) compiled a present-day tectonic stress map for eastern Asia region. The same stress field pattern confirms our study method and data used. But the stress filed inferred in this study covers more areas. The stress field obtained in this study is also consistent with GPS measurement (Wang et al, 2001; Wang et al, 2003) and its strain rate field (Shen et al, 2003; Zhang et al, 2004), quaternary fault slip rates and GPS observations (Holt et al, 2000), as well as GPS, geologic, and shear wave splitting data (Flesh et al, 2005).

Existence of the broad-scale radial pattern of σ_1 directions indicates that the primary force responsible for the tectonic movement and earthquake generation in continental area of China does not come from some local sources but from an external driving force on a large scale. It is quite likely related to the indentation effect of plate collision between India and Euroasia, as studied by many authors (e.g., Tapponnier and Molnar, 1976; Houseman and England, 1986; England and Houseman, 1986).

As mentioned previously, we have studied a stress field in some crustal volume which has a thickness represented by earthquake focal depth. Due to the limited resolving capability of the method and data that we used, we can say nothing about possible variation of the stress state with depth.

Most of stress relief measurement data are measured in shallow part of the crust. Strictly speaking, they cannot be used to invert the stress field in the deep part of the crust (e.g., Xu, 2001) for being affected by topography. In this study, we want to get the average stress field in a relatively large area, the topographic effect may be smoothed, so this sort of data can be used to constrain the stress field.

In the stress filed inversion, we select the data within the square areas of 5°×5° with the center of grid point. So the smoothing stress field can be achieved, and can be conveniently used to constrain the stress field in geodynamic process simulation, earthquake prediction (e.g., Peng et al, 2000; Wan, 2004) as well as slip property of active fault determination (Wan et al, 2008).

Acknowledgements This work is supported by the National Natural Science Foundation of China (40874022), Public Utility Research Project (200808053) and 973 program (2008CB425703). We would like to thank John Gephart for making his program available and Furen Xie for making Chinese stress field data available. Profs. Zhonghuai Xu and Zhengkang Shen provided their constructive comments and suggestions. The reviewers' comments improved the manuscript a lot.

References

Aki K (1966). Earthquake generating stress in Japan for the years 1961 to 1963 obtained by smoothing the first motion patterns. *Bull Earthq Res Inst* **44**: 447–471.

Angelier J (1979). Determination of the mean principal direction of stress for a given population. *Tectonophysics* **56**: T17–T26.

Angelier J (1989). From orientation to magnitudes in paleostress determination using fault slip data. *J Struct Geol* **11**: 37–50.

Cui X F and Xie F R (1999). Preliminary research to determine stress districts from focal mechanism solutions in Southwest China and its adjacent area. *Acta Seismologica Sinica* **12**(5): 562–572.

Du X X and Shao H C (1999). Modern tectonic stress field in the Chinese mainland inverted from focal mechanism solutions. *Acta Seismologica Sinica* **12**(4): 390–397.

England P C and Houseman G A (1986). Finite strain calculations of continental deformation 2, comparison with the India-Asia collision zone. *J Geophys Res* **91**: 3 664–3 676.

Flesch L M, Holt W E, Silver P G, Stephenson M, Wang C Y and Chan W W (2005). Constraining the extent of crust–mantle coupling in central Asia using GPS, geologic, and shear wave splitting data. *Earth Planet Sci Lett* **238**: 248–268

Gephart J W (1990). FMSI: A fortran program for inverting fault/slickenside and earthquake focal mechanism data to obtain the original stress tensor. *Comput Geosci* **16**: 953–989.

Gephart J W and Forsyth D W (1984). An improved method for determining the regional stress tensor using focal mechanism data: application to the San Fernando earthquake sequence. *J Geophys Res* **89**(B11): 9 305–9 320.

Gillard D, Wyss M and Okubo P (1996). Type of faulting and orientation of stress and strain as a function of space and time in Kilauea's south flank, Hawaii. *J Geophys Res* **101**: 16 025–16 042.

Hardebeck J L and Hauksson E (2001). Stress orientations obtained from earthquake focal mechanisms: what are appropriate uncertainty estimates? *Bull Seism Soc Amer* **91**: 250–262.

Holt W E, Chamot-Rooke N, Le Pichon X, Haines A J, Shen-Tu B and Ren J (2000). Velocity field in Asia inferred from Quaternary fault slip rates and global positioning system observations. *J Geophys Res* **105**: 19 185–19 209.

Horiuchi S, Russo G and Hasegawa A (1995). Discrimination of fault planes from auxiliary planes based on simultaneous determination of stress tensor and a large number of fault plane solutions. *J Geophys Res* **100**: 8 327–8 338.

Houseman G A and England P C (1986). Finite strain calculations of continental deformation 1, method and general results for convergent zones. *J Geophys Res* **91**: 3 651–3 663.

Kang Y, Yang X, Chen X, Chen G M and Zheng S H (2008). Inversion of stress field in Guangdong and its adjacent area. *Acta Seismologica Sinica* **21**(1): 58–66.

Li Q Z, Wang Z G, Chia Y N and Chin Y M (1973). Stress field obtained for two regions from weak earthquake data recorded at a single station. *Chinese J Geophys* **16**: 49–61 (in Chinese with English abstract).

Lu Z and Wyss M (1996). Segmentation of the Aleutian plate boundary derived from stress direction estimates based on fault plane solutions. *J Geophy Res* **101:** 803–816.

Lu Z, Wyss M and Pulpan H (1997). Details of stress directions in the Alaska subduction zone from fault plane solutions. *J Geophy Res* **102**: 5 385–5 402.

Michael A J (1984). Determination of stress from slip data: faults and folds. *J Geophy Res* **89**: 11 517–11 526.

Michael A J (1987). Use of focal mechanisms to determine stress: a control study. *J Geophys Res* **92**: 357–368.

Peng K Y, Yin X C, Wang H T and Zhang Y X (2000). Study on loading/unloading response ratio based on the tectonic stress field. *Earthquake Research in China* **16**(2): 190–196 (in Chinese with English abstract).

Shen Z K, Wang M, Gan W J and Zhang Z S (2003). Contemporary tectonic strain rate field of Chinese continent and its geodynamic implications. *Earth Science Frontiers* **10**(Suppl): 93–100 (in Chinese with English abstract).

Tapponnier P and Molnar P (1976). Slip-line field theory and large scale continental tectonics. *Nature* **294**: 319–324.

Wan Y G (2004). Some considerations on theory of load and unload response ratio and its application to earthquake prediction. *Northwestern Seismological Journal* **26**(2): 178–181 (in Chinese with English abstract).

Wan Y G, Shen Z K, Diao G L, Wang F C, Hu X L and Sheng S Z (2008). An algorithm of fault parameter determination using distribution of small earthquakes and parameters of regional stress field and its application to Tangshan earthquake sequence. *Chinese J Geophys* **51**(3): 569–583.

Wang M, Shen Z K, Niu Z J, Sun H R, Gan W J, Wang Q and Ren Q (2003). Contemporary crustal deformation of the Chinese continent and tectonic block model. *Science in China* (*Series D*) **33**(Suppl): 21–32 (in Chinese).

Wang Q, Zhang P Z, Freymueller J, Bilham R, Larson K, Lai X, You X, Niu Z, Wu J, Li Y, Liu J, Yang Z and Chen Q (2001). Presentday crustal deformation in China constrained by Global Positioning System (GPS) measurements. *Science* **294**: 574–577.

Wang S Y and Xu Z H (1985). Seismo-tectonic stress field in east China. *Acta Seismologica Sinica* **7**(1): 17–32 (in Chinese with English abstract).

Wyss M, Liang B, Tanigawa W R and Wu X (1992). Comparison of orientations of stress and strain tensors based on fault plane solutions in Kaoiki Hawaii. *J Geophys Res* **97**: 4 769–4 790.

Wyss M and Lu Z (1995). Plate boundary segmentation by stress directions: southern San Andreas fault, California. *Geophys Res Lett* **22**: 547–550.

Xie F R, Chen Q C, Cui X F, Li H, Yang S X, Guo Q L, Chen L W, Xu Z H, Zhang Y S, Dou S Q, Zhao J T, Zhang Z S, Liu C Y and Wang G J (2003). Database of crustal stress in China and its adjacent areas. In: Chen Q C, Cui X F, Li H, Yang S X and Chen L W eds. *Crustal Stress in China*. Geological Press, Beijing, 3–12 (in Chinese with English abstract).

Xie F R, Cui X F, Zhao J T, Chen Q C and Li H (2004). Regional division of the recent tectonic stress field in China and adjacent areas. *Chinese J Geophys* **47**(4): 654–662 (in Chinese with English abstract).

Xie F R, Zhu J Z, Liang H Q and Liu G X (1993). Basic characteristics of recent tectonic stress field in southwest China. *Acta Seismologica Sinica* **6**(4): 843–855.

Xu Z H (2001). A present-day tectonic stress map for Eastern Asia region. *Acta Seismologica Sinica* **14**(5): 524–533.

Xu Z H and Ge S M (1984). Stress field in the Fuyun, Xinjiang earthquake fracture zone determined by fitting fault slip vector data. *Acta Seismologica Sinica* **6**(4): 395–404 (in Chinese with English abstract).

Xu Z H, Wang S Y, Huang Y R and Gao A J (1992). Tectonic stress field of China inferred from a large number of small earthquakes. *J Geophys Res* **97**: 11 867–11 877.

Xu Z H, Wang S Y, Huang Y R, Gao A J, Jin X F and Chang X D (1987). Directions of mean stress axes in southwestern China deduced from microearthquake data. *Chinese J Geophys* **30**(5): 476–486 (in Chinese).

Xu Z H, Yan M and Zhao Z H (1983). Evaluation of direction of tectonic stress in North China from recorded data of a large number of small earthquakes. *Acta Seismologica Sinica* **5**(3): 268–279.

Xue H Y and Yan J Q (1984). The contemporary stress field around the Ordos block. *Chinese J Geophys* **27**(2): 144–152 (in Chinese with English abstract).

Zhang P Z, Shen Z K, Wang M, Gan W J, Buergmann R, Molnar P, Wang Q, Niu Z J, Sun J Z, Wu J C, Sun H R and You X Z (2004). Continuous deformation of the Tibetan Plateau from global positioning system data. *Geology* **32**(9): 809–812.

Zoback M L (1992). First and second order patterns of stress in the lithosphere: the world stress map project. *J Geophys Res* **97**(B8): 11 703–11 728.